International Journal of Material Science & Engineering– IJMSE
Volume 2 : Issue 1 [ISSN : 2374-149X]
Publication Date : 30 April, 2015

A finite element method to describe the cyclic behavior of saturated soil

[Tomohide Takeyama, Shinya Tachibana, Aiko Furukawa]

***Abstract*—In this paper, a finite element code to describe the cyclic behavior of saturated soil was developed. In order to describe the cyclic behavior, the EC model with the extended subloading surface, the rotational hardening and the hardening / softening due to shear was incorporated in the code as the constitutive model. The simulation of the cyclic simple shear test was carried out to validate the developed code and it was confirmed that the reasonable cyclic behavior of soil could be simulated.**

***Keywords*—finite element method, saturated soil, soil-water coupled problem, cyclic behavior, liquefaction**

I. Introduction

The saturated sandy soil is mixed material of soil grain and pore water. The volume change due to shear which is called dilatancy is the important mechanical characteristics of granular materials. The liquefaction of sandy soil is deeply retated to the dilatancy. When the cyclic shear stress due to an earthquake is subjected to loosely deposited saturated sandy soil, the soil would contract by the negative dilatancy. However the volume change is constrained by the pore water, pore water pressure rises and the effective stress decreases. When the effective stress become zero and the shear strength is disappeared, the soil is liquefied. This is the mechanism of the liquefaction of the sandy soil. The liquefaction have been estimated by mainly two methods so far. The first one is the simple method using the liquefaction strength and the safety factor for liquefaction based on the laboratory tests on the sandy soil. the other is the dynamic analyses based on the total stress. Nowadays, the dynamic analyses based on the effective stress that the deformation of the soil structure and the seepage of the pore water have been developed.

Tomohide Takeyama
Tokyo Institute of Technology
Japan

Shinya Tachibana
Saitama University
Japan

Aiko Furukawa
Kyoto University
Japan

The objective of this research is to formulate the mechanical behavior of the soil structure and the pore water as the initial and boundary problem in the field considering the acceleration due to an earthquake and to develop the soil-water coupled dynamic finite element method. In this research, the EC model[1][2][3] with the extended subloading surface[4][5], the rotational hardening[6] and the hardening / softening due to shear[7] is employed as the constitutive model to describe especially the dilatancy due to the cyclic shear stress.

II. Finite Element Formulation of Soil-water Coupled Dynamic Problem

The governing equations to describe the soil-water coupled dynamic problem are as follows. In the following description, compression is defined to be positive.

$$\rho\ddot{\mathbf{u}} + \nabla\cdot\boldsymbol{\sigma} - \rho\mathbf{b} = 0 \tag{1}$$

$$\boldsymbol{\sigma} = \boldsymbol{\sigma}' + p_w\mathbf{1} \tag{2}$$

$$\dot{\boldsymbol{\sigma}}' = \mathbf{C} : \dot{\boldsymbol{\varepsilon}} \tag{3}$$

$$\boldsymbol{\varepsilon} = -\left(\mathbf{u}\otimes\nabla + \nabla\otimes\mathbf{u}\right)/2 \tag{4}$$

$$\dot{\mathbf{w}} = -\mathbf{k}\cdot\nabla h \tag{5}$$

$$\dot{\varepsilon}_v - \nabla\cdot\dot{\mathbf{w}} - \left(n\dot{p}_w\right)/K_w \tag{6}$$

Equations (1) to (6) are the equation of motion, the principal of effective stress, the constitutive equation, the strain-displacement relation, the Darcy's law and the continuity equation respectively. ρ is density, $\mathbf{u}$ is displacement vector, $\boldsymbol{\sigma}$ is stress tensor, $\mathbf{b}$ is body force vector, $\boldsymbol{\sigma}'$ is effective stress tensor, p_w is pore water pressure, $\mathbf{1}$ is Kroneker's delta, $\mathbf{C}$ is constitutive tensor, $\boldsymbol{\varepsilon}$ is strain tensor, $\mathbf{w}$ is Darcy's velocity, $\mathbf{k}$ is hydraulic conductivity tensor, h is total water head, ε_v is volumetric strain, n is porosity, K_w is bulk modulus of pore water. The boundary conditions are

$$\hat{\mathbf{u}} = \mathbf{u} \quad \text{on } S_u \tag{7}$$

$$\hat{\mathbf{t}} = \boldsymbol{\sigma}^T\cdot\mathbf{n} \quad \text{on } S_\sigma \tag{8}$$

$$\hat{h} = h \quad \text{on } S_h \tag{9}$$

$$\hat{q} = \mathbf{w} \cdot \mathbf{n} \quad \text{on } S_q \tag{10}$$

where **t** is traction vector, **n** is normal vector to the boundary surface, q is quantity of flowing pore water, S_u is displacement boundary, S_σ is stress boundary, S_h is head boundary, S_q is flow boundary.

By multiplying the rate form of equation of motion (1) by a test function $\delta\dot{\mathbf{u}}$ and volume integrating it, the weak form of equation is obtained:

$$\begin{aligned}&\int_V \rho\delta\dot{\mathbf{u}}\cdot\ddot{\mathbf{u}}dV + \int_V \dot{\rho}\delta\dot{\mathbf{u}}\cdot\dot{\mathbf{u}}dV + \int_V \delta\dot{\boldsymbol{\varepsilon}}\cdot\dot{\boldsymbol{\sigma}}'dV \\ &+\int_V \delta\dot{\varepsilon}_v \dot{p}_w dV - \int_{S_\sigma} \delta\dot{\mathbf{u}}\cdot\hat{\mathbf{t}}dS - \int_V \rho\delta\dot{\mathbf{u}}\cdot\dot{\mathbf{b}}dV \\ &-\int_V \dot{\rho}\delta\dot{\mathbf{u}}\cdot\mathbf{b}dV = 0\end{aligned} \tag{11}$$

The weak form of the continuity equation is obtained by the same procedure:

$$\begin{aligned}&\int_V \delta h\dot{\varepsilon}_v dV - \int_{S_q} \delta h\hat{q}dS + \int_V (\nabla\delta h)\cdot\dot{\mathbf{w}}dV \\ &-\int_V \delta h\frac{n}{K_w}\dot{p}_w dV = 0\end{aligned} \tag{12}$$

The field variables are spatially discretized as shown below

$$\{u\} = [N]\{u^{ne}\},\ \{\varepsilon\} = [B]\{u^{ne}\},\ \{\varepsilon_v\} = [B_v]\{u^{ne}\}, \tag{13}$$

$$h = [N_h]\{h^{me}\},\ \{\nabla h\} = [B_h]\{h^{me}\}, \tag{14}$$

where $[N]$, $[B]$, $[B_v]$, $[N_h]$ and $[B_h]$ are the shape function matrices, the super script *ne* and *me* indicate the variables at the discretized points. By substituting (13) and (14) to (11) and (12), the spatially discretized weak forms of the equation of motion and the continuity equation of an element are obtained:

$$\begin{aligned}&[M^e]\{\ddot{u}^{ne}\} + \{[C_M^e] + [C_R^e]\}\{\ddot{u}^{ne}\} \\ &+[K^e]\{\dot{u}^{ne}\} + [K_v^e]^T\{\gamma_w\dot{h}^{me}\} = \{\dot{F}^e\}\end{aligned} \tag{15}$$

$$[K_v^e]\{\dot{u}^{ne}\} - [K_{h1}^e]\{\gamma_w h^{me}\} - [K_{h2}^e]\{\gamma_w\dot{h}^{me}\} = \{\dot{Q}^e\} \tag{16}$$

where the matrices are expressed as follows:

$$[M^e] = \int_{V^e} \rho[N]^T[N]dV \tag{17}$$

$$[C_M^e] = \int_{V^e} \dot{\rho}[N]^T[N]dV \tag{18}$$

$$[K^e] = \int_{V^e} [B]^T[D][B]dV \tag{19}$$

$$[K_v^e] = \int_{V^e} [N_h]^T[B_v]dV \tag{20}$$

$$[K_{h1}^e] = \int_{V^e} [B_h]^T\frac{[k]}{\gamma_w}[B_h]dV \tag{21}$$

$$[K_{h2}^e] = \int_{V^e} (n/K_w)[N_h]^T[N_h]dV \tag{22}$$

$$\begin{aligned}\{\dot{F}^e\} &= \int_{S_\sigma^e} [N]^T\{\hat{t}\}dS + \int_{V^e} \rho[N]^T\{\dot{b}\}dV \\ &+\int_{V^e} \dot{\rho}[N]^T\{b\}dV\end{aligned} \tag{23}$$

$$\{\dot{Q}^e\} = \int_{S_q^e} [N_h]^T\{\hat{q}\}dS \tag{24}$$

$[C_R^e]$ is the Rayliegh damping matrix and is represented as

$$[C_R^e] = \alpha_0[M^e] + \alpha_1[K^e] \tag{25}$$

where α_0 and α_1 are the constants. The acceleration, velocity and displacement in equations (15) and (16) are temporally discretized by Newmark method:

$$\ddot{\mathbf{u}}_{t+\Delta t} = \ddot{\mathbf{u}}_t + \Delta t\dddot{\mathbf{u}}_{t+\Delta t} \tag{26}$$

$$\dot{\mathbf{u}}_{t+\Delta t} = \dot{\mathbf{u}}_t + \Delta t\ddot{\mathbf{u}}_t + \gamma\Delta t(\ddot{\mathbf{u}}_{t+\Delta t} - \ddot{\mathbf{u}}_t) \tag{27}$$

$$\mathbf{u}_{t+\Delta t} = \mathbf{u}_t + \Delta t\dot{\mathbf{u}}_t + (\Delta t^2/2)\ddot{\mathbf{u}}_t + \beta\Delta t^2(\ddot{\mathbf{u}}_{t+\Delta t} - \ddot{\mathbf{u}}_t) \tag{28}$$

The equations (15) and (16) are solved iteratively. Describing the increment of acceleration, velocity and displacement during iterative calculation as $\Delta\ddot{\mathbf{u}}^{(k+1)}$, $\Delta\dot{\mathbf{u}}^{(k+1)}$ and $\Delta\mathbf{u}^{(k+1)}$, the following equations are obtained from equations (26), (27) and (28):

$$\dddot{\mathbf{u}}_{t+\Delta t}^{(k+1)} = \dddot{\mathbf{u}}_{t+\Delta t}^{(k)} + \Delta\ddot{\mathbf{u}}^{(k+1)}/\Delta t \tag{29}$$

$$\ddot{\mathbf{u}}_{t+\Delta t}^{(k+1)} = \ddot{\mathbf{u}}_{t+\Delta t}^{(k)} + \Delta\ddot{\mathbf{u}}^{(k+1)} \tag{30}$$

$$\dot{\mathbf{u}}_{t+\Delta t}^{(k+1)} = \dot{\mathbf{u}}_{t+\Delta t}^{(k)} + \gamma\Delta t\Delta\ddot{\mathbf{u}}^{(k+1)} \tag{31}$$

$$\mathbf{u}_{t+\Delta t}^{(k+1)} = \mathbf{u}_{t+\Delta t}^{(k)} + \beta\Delta t^2\Delta\ddot{\mathbf{u}}^{(k+1)} \tag{32}$$

The superscript with bracket indicates iteration count. The initial values of the iteration are set to be

$$\dddot{\mathbf{u}}_{t+\Delta t}^{(0)} = 0 \tag{33}$$

$$\ddot{\mathbf{u}}_{t+\Delta t}^{(0)} = \ddot{\mathbf{u}}_t \tag{34}$$

$$\dot{\mathbf{u}}_{t+\Delta t}^{(0)} = \dot{\mathbf{u}}_t + \Delta t\ddot{\mathbf{u}}_t \tag{35}$$

$$\mathbf{u}_{t+\Delta t}^{(0)} = \mathbf{u}_t + \Delta t\dot{\mathbf{u}}_t + (\Delta t^2\ddot{\mathbf{u}}_t)/2. \tag{36}$$

The total water head and the time derivative of the total water head in equation (15) and (16) are temporally discretized as

$$h = (1-\theta)h_t + \theta h_{t+\Delta t} \tag{37}$$

$$\dot{h} = (h_{t+\Delta t} - h_t)/\Delta t \tag{38}$$

where θ is constant within a range from 0 to 1. By substituting the equations (29), (30), (31), (32), (37) and (38) to the equations (15) and (16), and summing up all elements, the spatially and temporally discretized weak forms of the equation of motion and the continuity equation (The global stiffness equations) are obtained:

$$\begin{aligned}&\left[[M]+\Delta t[C]+\gamma\Delta t^2[K]\right]\left\{\Delta\ddot{u}^{n(k+1)}\right\}+[K_v]^T\left\{\gamma_w h^m_{t+\Delta t}\right\}\\&=\Delta t\left\{\dot{F}\right\}-\Delta t[M]\left\{\ddot{u}^{n(k)}\right\}-\Delta t[C]\left\{\ddot{u}^{n(k)}\right\}\\&-\Delta t[K]\left\{\dot{u}^{n(k)}\right\}+[K_v]^T\left\{\gamma_w h^m_t\right\}\end{aligned} \tag{39}$$

$$\begin{aligned}&\gamma\Delta t^2[K_v]\left\{\Delta\ddot{u}^{n(k+1)}\right\}-\left[\theta\Delta t[K_{h1}]+[K_{h2}]\right]\left\{\gamma_w h^m_{t+\Delta t}\right\}\\&=\Delta t\left\{\dot{Q}\right\}-\Delta t[K_v]\left\{\dot{u}^{n(k)}\right\}\\&+(1-\theta)\Delta t[K_{h1}]\left\{\gamma_w h^m_t\right\}-[K_{h2}]\left\{\gamma_w h^m_t\right\}\end{aligned} \tag{40}$$

III. Constitutive Model to Describe Cyclic Behavior of Soil

In order to describe the cyclic behavior of soil, the constitutive model employed in this research is the EC model with the extended subloading surface, the rotational hardening and the hardening / softening due to shear which are explained later. Sekiguchi and Ohta (1977)[8] developed their model assuming that the volumetric change of normally consolidated clays due to contractancy (negative dilatancy) and the stress ratio exhibits linear relationship based on Shibata's (1963)[9] drained shear tests under conditions of constant effective mean stress. However, this does not preclude other nonlinear functions, such as exponential and/or logarithmic curves. Ohno, Iizuka and Ohta (2006)[1], Ohno, Takeyama, Pipatpongsa, Iizuka and Ohta (2007)[2] and Ohta, Iizuka and Ohno (2011)[3] proposed two categories of elasto-plastic model in which (original) Cam Clay, Modified Cam Clay and Sekiguchi-Ohta models are included as special cases. They characterize the relationship between the contractancy and the stress ratio using either exponential or logarithmic function and named EC model, LC model respectively which are collectively named the Extended Sekiguchi-Ohta model.

The yield function of EC model is

$$f = \mathrm{M}D\ln\frac{p'}{p'_0} + \frac{\mathrm{M}D}{n_E}\left(\frac{\eta^*}{\mathrm{M}}\right)^{n_E} - \varepsilon_v^p = 0 \tag{41}$$

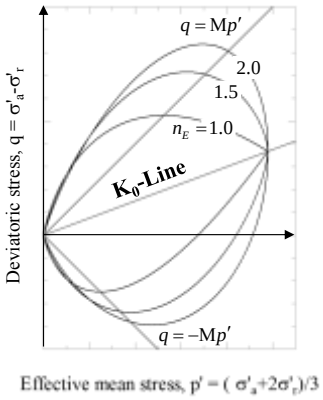

Figure 1. Yield surface of the EC model in axi-symmetric stress plane.

in which M is critical state parameter; D is coefficient of dilatancy proposed by Shibata (1963)[9]; p' is effective mean principal stress; η^* is generalized stress ratio (Sekiguchi and Ohta 1977[8]) described as

$$\eta^* = \sqrt{\frac{3}{2}}\left\|\boldsymbol{\eta} - \boldsymbol{\eta}_0\right\| \tag{42}$$

in which $\boldsymbol{\eta}$ is stress ratio tensor which is stress deviator $\mathbf{s}$ divided by p'. The subscript 0 indicates the preconsolidated state. n_E is the parameter describing the nonlinearity of the constractancy and the stress ratio curve. The EC model is identical to the Sekiguchi-Ohta model when n_E = 1.0. The yield surfaces of EC model expressing in variation with the values of n_E are depicted in Fig. 1.

During the earthquake, the shear deformation occurs in the ground and the pore water pressure arises due to the contractancy. Thus the effective mean stress decreases. And then the liquefaction occurs when the effective mean stress becomes 0. Therefore it is need that the constitutive model can represent at least the decrease of the effective mean stress in undrainage shear deformation by cyclic load. However, the constitutive model which I mentioned above cannot represent this feature. In order to represent this feature, the subloading surface proposed by Hashiguchi et al. (1998)[7] is employed in this research. The subloading surface is always inside the normal yield surface and the current stress is on the subloading surface. The plastic strain is developed although the stress is inside the normal yield surface by applying subloading surface. Therefore the reduction of effective pressure due to cyclic load can be calculated. The function of subloading surface is as follows.

$$f = \mathrm{M}D\ln\frac{p'}{p'_0} + \frac{\mathrm{M}D}{n_E}\left(\frac{\eta^*}{\mathrm{M}}\right)^{n_E} - \varepsilon_v^p - \mathrm{M}D\ln R = 0 \tag{43}$$

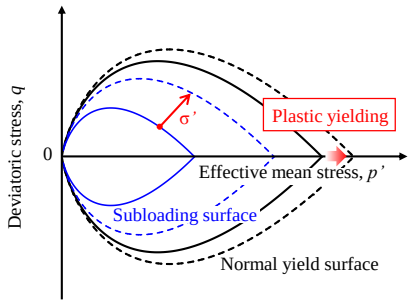

Figure 2. Subloading surface and normal yield surface

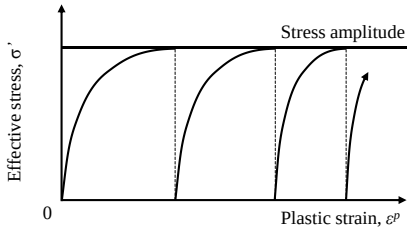

Figure 3. Cyclic loading behavior by subloading surface model

$R = p'_y / p'_c$ is called the similarity ratio of subloading surface which indicates the ratio of size between the subloading surface and normal yield surface. The subloading surface and the normal yield surface on axi-symmetric stress plane are shown in Fig. 2. The similarity ratio R changes according to the developing law which is proposed by Hashiguchi et al. (1998)[7]:

$$\dot{R} = -\frac{m}{D} \ln R \left\| \dot{\boldsymbol{\varepsilon}}^p \right\| \tag{44}$$

where m is the parameter which controls the speed of the subloading surface to achieve the normal surface.

The stress-strain curve of cyclic behavior simulated by using subloading surface model is opened loop as shown in Fig. 3. Therefore the accumulation of plastic strain due to cyclic loading is overestimated. Hashiguchi (1980[4], 1989[5]) was proposed the extended subloading surface model to overcome this problem. In addition to the extended subloading surface model, the rotational hardening model proposed by Hashiguchi (1977)[6] is also employed by replacing the tensor expressing the anisotropy $\boldsymbol{\eta}_0$ with the variable $\boldsymbol{\eta}_e$. The function of extended subloading surface is expressed as

$$f = \mathrm{M}D \ln \frac{\bar{p}'}{p'_0} + \frac{\mathrm{M}D}{n_E} \left(\frac{\bar{\eta}^*}{\mathrm{M}} \right)^{n_E} - \varepsilon_v^p - \mathrm{M}D \ln R = 0 . \tag{45}$$

The modified effective stress is defined as $\bar{\boldsymbol{\sigma}}' = \boldsymbol{\sigma}' - (1-R)\boldsymbol{\alpha}$ where $\boldsymbol{\alpha}$ is similarity center of the subloading surface. In the case that the similarity center is set to be the origin, that is $\boldsymbol{\alpha}$ = 0, the extended subloading surface is identical to the subloading surface. The modified mean effective stress and the modified generalized stress ratio are

$$\bar{p}' = tr(\bar{\boldsymbol{\sigma}}')/3 \tag{46}$$

$$\bar{\eta}^* = \sqrt{\frac{3}{2}} \left\| \bar{\boldsymbol{\eta}} - \boldsymbol{\eta}_e \right\| \tag{47}$$

in which $\bar{\boldsymbol{\eta}}$ is the modified stress ratio tensor which is modified stress deviator $\bar{\mathbf{s}}$ divided by $\bar{p}'$. The developing law of $\boldsymbol{\alpha}$ and $\boldsymbol{\eta}_e$ are

$$\dot{\boldsymbol{\alpha}} = c \left\| \dot{\boldsymbol{\varepsilon}}^p \right\| (\boldsymbol{\sigma}' - \boldsymbol{\alpha}) + \frac{1}{p'_c} \left\{ \dot{p}'_c - \dot{\boldsymbol{\eta}}_e \frac{\partial f\left(p'_\alpha, \eta^*_\alpha\right)}{\partial \boldsymbol{\eta}_e} \right\} \boldsymbol{\alpha} \tag{48}$$

$$\dot{\boldsymbol{\eta}}_e = b_r \left\{ m_r (\boldsymbol{\eta} - \boldsymbol{\eta}_e) - \left\| \boldsymbol{\eta} - \boldsymbol{\eta}_e \right\| \boldsymbol{\eta}_e \right\} \left\| \dot{\boldsymbol{\varepsilon}}_d^p \right\| \tag{49}$$

where c is the parameter which controls the speed of the similarity center; b_r is the parameter which controls the rotational speed of the yield surface; M_r is the parameter which defined the rotational limit of the yield surface. Figs. 4 and 5 schematically shows the hardening due to the movement / expansion of the extended subloading surface and the rotation of the normal yield surface.

It was reported by Castro (1969)[10], Tatsuoka (1972)[11] etc. that the hardening of the sandy soil is not only caused by plastic volumetric change but also the plastic shear distortion. Hashiguchi and Chen (1998)[6] was proposed the hardening / softening due to shear to describe this experimental results in the numerical simulation. The developing law of the hardening parameter H is

$$\dot{H} = \dot{\varepsilon}_v^p + \sqrt{\frac{2}{3}} \mu \left\| \dot{\boldsymbol{\varepsilon}}_d^p \right\| (\eta - \mathrm{M}_d) . \tag{50}$$

μ is the parameter which controls the contribution of the hardening / softening due to shear. M_d is the parameter which define the boundary of the hardening and softening. Fig. 6 schematically shows the hardening / softening due to shear in p' - q stress plane.

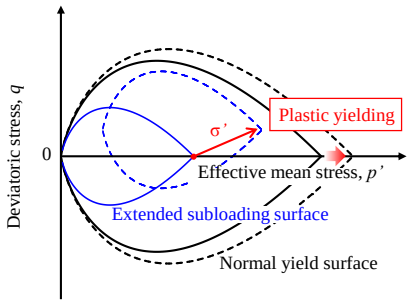

Figure 4. hardening due to the movement / expansion of the extended subloading surface

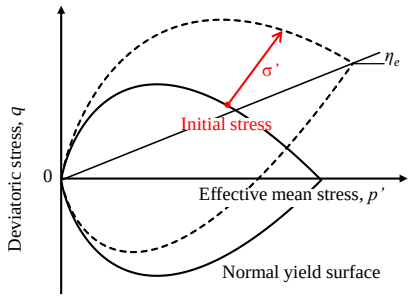

Figure 5. hardening due to the rotation of the normal yield surface

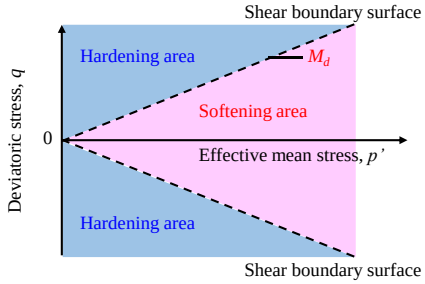

Figure 6. Hardening / softening due to shear

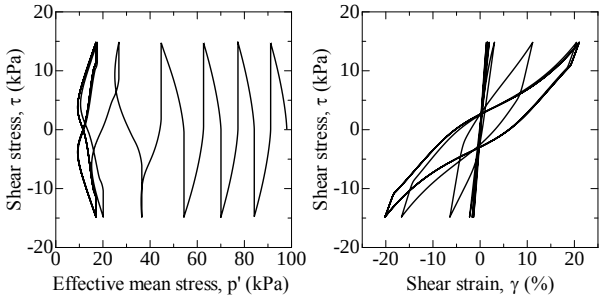

Figures 7. Simulated effective stress path and stress-strain relationship

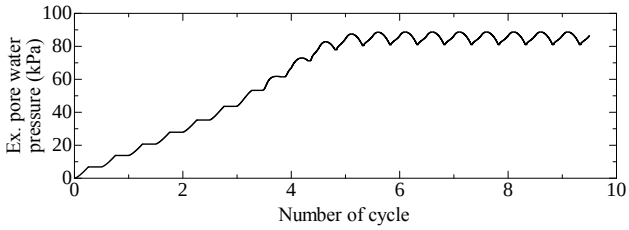

Figure 8. Excess pore water pressure vs. number of cycle

IV. Numerical Examples

In order to validate the F.E. code, the simulation of the cyclic simple shear test is carried out. The amplitude of the shear stress is constant of 14.8kPa. The constitutive model mentioned in the chapter III is employed in this simulation. The material parameters used in the simulation are listed in Table I. Figs. 7 show the simulated stress path and the simulated stress-strain relationship. The reduction of effective mean stress due to cyclic load can be simulated as shown in Fig. 7. The reduction of the shear modulus during cyclic deformation also can be seen in Fig. 7. The excess pore water pressure versus the number of cycle is shown in Fig. 8. It can be seen that the liquefaction almost occurs after fifth time of cycle.

TABLE I. MATERIAL PARAMETERS USED IN THE SIMULATION

Coefficient of dilatancy	D		0.051
Irreversibility ratio	Λ		0.697
Critical stress parameter	M		1.22
Poisson's ratio	ν'		0.344
Parameter for EC model	n_E		1.4
Parameter for subloading surface	m		0.1
Parameter for extended subloading surface	c		30.0
Parameter for rotational hardening	b_r		1.0
	M_r		0.8
Parameter for hardening / softening due to shear	μ		2.0
	M_d		0.8
Initial effective mean stress	p'_i	(kPa)	98.0
Preconsolidated effective mean stress	P'_0	(kPa)	98.0

V. Conclusions

In this research, the mechanical behavior of the soil structure and pore water in the field considering the acceleration due to an earthquake was formulated as the initial and boundary problem and the soil-water coupled dynamic F.E. code was developed employing the EC model with the extended subloading surface, the rotational hardening and the hardening / softening due to shear as the constitutive model. The cyclic simple shear test was carried out by the developed code and it was confirmed that the reduction of effective stress and accumulation of the excess pore water pressure due to the cyclic load could be seen.

The developed F.E. code will be incorporated in IES (Integrated Earthquake Simulator) which is developing to predict the seismic motion and damage by the K computer which is a super computer installed at the RIKEN Advanced Institute for Computational Science in Kobe, Japan.

Acknowledgment

This work is supported in part by the grant from RIKEN, Advanced Institute for Computational Science.

References

[1] Ohno, S., Iizuka, A. and Ohta, H., "Two categories of new constitutive model derived from non-linear description of soil contractancy," J. Applied Mech., JSCE 9: pp. 407-414 (in Japanese), 2006.

[2] Ohno, S., Takeyama, T., Pipatpongsa, T., Iizuka, A. and Ohta, H., "Analysis of embankment by nonlinear contractancy description," Proc. 13th Asian Regional Conf. of Soil Mechanics and Geotechnical Engineering, Kolkata, December 2007.: pp. 1097-1100, 2007.

[3] Ohno, S., Takeyama, T., Pipatpongsa, T., Iizuka, A. and Ohta, H., "Analysis of embankment by nonlinear contractancy description," Proc. 13th Asian Regional Conf. of Soil Mechanics and Geotechnical Engineering, Kolkata, December 2007.: pp. 1097-1100, 2007.

[4] Hashiguchi, K., "Constitutive equations of elastoplastic materials with elastic-plastic transition," Journal of Applied Mechanics ASME Vol.47, pp. 266-272., 1980.

[5] Hashiguchi, K., "Subloading surface model in unconventional plasticity," Int. J. Solids Struct. Vol.25, pp.917-945, 1989.

[6] Hashiguchi, K., "An expression of anisotropy in a plasitc consititutive equation of soils," Proc. of the 9th Int. Conf. Soil Mech. and Foundation Eng., pp.302-305, 1977.

[7] Hashiguchi, K. and Chen, Z.P., "Elastoplastic constitutive equation of soils with the subloading surface and rotational hardening," Int. J. for Numerical and Analytical Methods in Geomechanics Vol. 22, pp.197-227, 1998.

[8] Sekiguchi, H. and Ohta, H., "Induced anisotropy and time dependency in clays," Proc. Specialty Session 9, 9th Int. Conf. Soil Mech. and Foundation Eng., pp. 306-315, 1977.

[9] Shibata, T., "On the volume changes of normally consolidated clays," Annual of Disaster Pevension Research Institute, Kyoto University (6): pp. 128-134, 1963.

[10] Castro, G., "Liquefaction of sands," Ph.D. Thesis, Harvard Soil Mech. Series No.81, 1969.

[11] Tatsuoka, F., "Study on deformation characteristics of sand by triaxial tests," Doctor Thesis, Tokyo University., 1972.